Effect of Gold Loading on Time-Resolved ps Photoluminescence of ZnO

Published as part of The Journal of Physical Chemistry virtual special issue "Cynthia Friend Festschrift".

A. Ziani, S. Al-Taweel, M. A. Nadeem, and H. Idriss*

ABSTRACT: Au/ZnO with Au at.% between 0.1 and 3.0, were prepared, analyzed by UV-vis, transmissio n electro n micro sco py(TEM), X-ray pho to electro nspectro sco py(XPS), and o ther techniques. The bandgap energy o f all materials was 3.3 eV, all sho wed a pro no uncedplasmo n reso nance at abo ut 2.5 eV when Au was present. Au depo sited on ZnO surfaces had a mean particle size between 2.7 and 4.4 nm (depending o n coverage), while ZnO particles had a mean size of 105 nm. XPS Au $4f_{7/2}$ indicated that Au is in its metallic state (binding energy at 83.8 ± 0.1 eV) in the investigated series. Time-resolved photoluminescence (TPRL) was conducted to monitor the band to band (e-h) reco mbinatio ndecay signal o n ZnO and Au/ZnO. The decay was best fitted w ith a biexponential function with time constants t_1 and t_2 ranging from 20 to 25 ps and from 57 to 85 ps, respectively, for the whole series with Au/ZnO showing faster decay rate than ZnO. Fitting the decay function followed by its integration over the investigated time domain then normalizing it with gold atoms provided a useful method to quantify the effect of Au particles on radiative recombination rates of ZnO. The resulting function showed a single exponential decay with respect to Au atoms on the surface of ZnO; $y(x) = A\exp(-ax)$, where x is the atomic % of Au on ZnO and $a = 2.4$. This indicated that charge trapping, per Au atom, is most efficient at very low coverage. Possible reasons for this and links to observed similar results in photocatalytic reactions on noble metal/semiconductors materials are discussed.

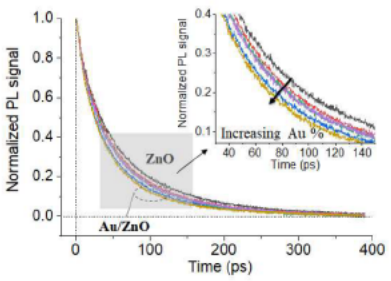

INTRODUCTION

Zinc oxide is an n-type semiconductor due to a small deviation from stoichiometry $ZnO_{1-\delta}$ ($\delta \ll 1$), with a band gap of about 3.4 eV at room temperature. It is a support for many catalytically relevant reactions, such as in Cu/ZnO catalysts for methanol synthesis, and is one of the most used catalysts in the chemical industry. It also has many other applications in optoelectronics and as electric sensors. Upon UV-light excitation, ZnO gives an intense near-band-edge emission in the UV (~375 nm) and a green emission in the visible region (~550 nm),[1] with the latter being associated with intrinsic defects, such as oxygen anion vacancies.[2]

Photoluminescence of ZnO powder and single crystals have been studied both by steady state and time-resolved methods for a few decades.[3−11] These studies have shed light onto many aspects of e-h recombination rates and the role of structural, electronic, and chemical (adsorbates) properties on the signal intensity and decay rates. Of particular interest is the interface metal−semiconductor, where in general the metal is deposited post-semiconductor synthesis, ensuring dispersion on its surface. Light interaction with such a system may alter both components depending on its energy and intensity. In that regard, materials based on coinage metals (Cu, Ag, and Au) dispersed on ZnO have received considerable attention because of their plasmonic resonance response to near-UV, visible, and IR light.[12−14] Noble metals, in general, alter ZnO response to light excitation because they act as electron trap centers due to their higher work function.[15]

A non-negligible amount of work was devoted to study the charge transfer between a plasmonic metal and ZnO using time-resolved spectroscopy, although mostly in the ns and longer periods. Considering the effect of the density of Au particles on ZnO, a decrease of the lifetime of the ns photoluminescence[16] was seen for Au coverage (with an average particle size of 14 nm) ranging between 1.7 and 9.2 wt % under UV excitation. However, an increase in the lifetime was seen when time-resolved experiments were conducted under continuous visible light excitation in addition. From these measurements the authors extracted a time constant for charge transfer from ZnO to Au of about 7.5×10^8 s^{-1}, which was almost the same time constant of electron transfer from Au particles to ZnO of 7.7×10^8 s^{-1}. Another work was devoted to the study of Au nanorods (70 nm long with a diameter of 20 nm) inside different sizes of ZnO particles (with shell

thicknesses ranging from about 30 to 60 nm).[17] The objective was to study the electron transfer effect on generating singlet molecular oxygen. Hot electrons generated within Au rods are injected into the conduction band (CB) of ZnO, which in turn are transferred to molecular oxygen to reduce it to the O_2^- radical. The then-formed radicals would get oxidized back by donating their electrons to Au particles with a higher probability of making singlet oxygen.

The effect of metals on top of ZnO on its photoluminescence intensity was studied by many authors, in addition. By creating an ordered pattern of Pt (of about 30 nm thick) containing ordered 3D-voids of about 500 nm in size (on top of 1 μm thick ZnO), a 12-fold enhancement on the UV emission was seen.[18] Moreover, the lifetime of the UV emission increased (instead of decreased) due to Pt. This was explained as due to the coupling of Pt surface plasmon with the e-h recombination radiative emission as well as a decrease of the nonradiative contribution of the decay rate because of the presence of Pt on the surface. Gold particles of about 5 nm in size deposited on top of ZnO rods (700 nm long with a diameter of 40 nm) resulted in a six times increase in the intensity of the UV emission; although their concentration is not mentioned, SEM images show high coverage.[19] In these experiments the light excitation wavelength was 258 nm. The lifetime was also measured and gold particles were found to decrease the decay rate of the radiative recombination from 130 (ZnO) to 90 ps (Au/ZnO). Given that the exciton (3.36 eV) energy is not resonant with the 5 nm Au NP (2.25 eV), the additional fast exciton relaxation pathway may involve a surface energy transfer (SET) mechanism. The authors thus proposed that ZnO exciton dipole nonradiatively transfers its energy via either a metallic surface Au interband excitation (Au 5d band to Au 6sp band) or a near surface Au conduction band electron. The transition lifetimes involved in this SET process are in the subps range,[20] much shorter than the ZnO exciton relaxation. Therefore, it is fast enough to provide an additional decay channel to increase the exciton spontaneous energy (due to dipole−dipole coupling between the exciton and Au plasmon) transfer rate and increase the UV emission. Two different coverages with Au particles of 30 nm in size over ZnO rods (10 μm long, with d = 0.15 μm) were also studied.[21] While focusing the SEM microscope on a single ZnO rod and conducting time-resolved photoluminescence study at the ns scale, it was found that the presence of Au particles decreased the UV emission intensity independently from the coverage (2 and 15% of the surface).

Many other works have addressed the same topic not mentioned above. It is, however, clear that only a small fraction of work are devoted to study the effect of small particles of Au about 3 nm in size (which is the size mostly relevant for catalytic reactions[22−25]) while linking their surface density to lifetime photoluminecence rates in the ps range.

In this work we have mostly focused on extracting the mean size of gold particles on top of ZnO by TEM, quantified their atomic percent on the surface of ZnO by XPS in view of analyzing their effect on the ZnO decay rate of the e-h recombination by time-resolved femto second photoluminescence.

EXPERIMENTAL DETAILS

Au/ZnO powders were prepared by the deposition precipitation method with urea (DPU) following procedures similar to those described by Zanella et al.[26] and Alonso et al.[27]

Briefly, $HAuCl_4 \cdot 3H_2O$, Sigma-Aldrich, (1.654 g) was dissolved in milli-Q water (1 L) to give a metal stock solution of concentration 4.2×10^{-3} mol L^{-1}. For example, for the preparation of 1 wt % Au/ZnO powder, 36.8 mL of the stock solution (diluted to 300 mL with milli-Q water), urea (7.50 g), and ZnO (3 g) were mixed under vigorous mechanical stirring, after which the solution was heated to 80 °C and held at this temperature for 8 h. The resulting powder was then collected by vacuum filtration, washed repeatedly with milli-Q, and then air-dried at 50 °C overnight. Following drying, the powder was calcined at 350 °C in static air for 2 h. The series of catalysts used for this work was prepared using the same method. That way, 0.1, 0.3, 0.5, 0.7, and 1 wt % Au deposited on ZnO catalysts were prepared. Zinc oxide was prepared from zinc nitrate solution ($Zn(NO_3)_2 \cdot 6H_2O$), Sigma-Aldrich, by precipitation with NH_4OH at RT at pH > 9, followed by washing with milli-Q water, filtration, drying in an oven at 80 °C overnight, and then calcined at 400 °C for 5 h in static air.

X-ray diffraction patterns of the samples were obtained using a Discovery Bruker diffractometer (with Cu $K_{\alpha 1}$ radiation). The data sets were acquired in continuous scanning mode over the 2θ range, 10−90°, using a step interval of 0.01° and a counting time of 2.0 s per step.

UV−visible reflectance (R) spectra were recorded using an Evolution 300 Thermo Scientific spectrometer in the 200−1000 nm wavelengths range using an integrating sphere attachment. $BaSO_4$ powder was used as a reference. For each sample, the absorbance α calculated from the reflectance using the relation $\alpha = -1/[\log_{10}(1/R)]$. The band gap energy of the material (E_g) is calculated assuming a direct allowed transition and applying the relation $\alpha(h\nu)^2 = h\nu - E_g$, where $h\nu$ is the photon energy. In the plot of $(h\nu)^2$ as a function of $h\nu$, the extrapolation of the linear region of the plot at zero gives the value of E_g.[28] More details on the different types of fitting can be found in ref 29.

Scanning transmission electron microscopy (STEM) studies were performed using Titan ST microscope (FEI company) operated at an accelerating voltage of 300 kV equipped with a field emission electron gun, a 4k × 4k CCD camera, a Gatan imaging filter (GIF) Tridiem, and the Gatan imaging software suite (Gatan Inc.). The microscope was operated in high angle annular dark field (HAADF)-STEM mode (Z-contrast) with point-to-point resolution of about 0.12 nm and the information limit of about 0.10 nm. To prepare samples for analysis, a spec of catalyst was dispersed in ethanol followed by ultrasonication of the mixture for 15 min. A drop of supernatant suspension was poured onto a holey carbon coated Cu grid placed on a filter paper and left to dry before the grid was loaded on a double tilt sample holder. Energy-dispersive X-ray (EDX) analysis was performed at a 14° sample holder tilt angle to maximize the X-ray collection and was used to confirm the Au particle assignment when needed.

XPS was conducted using a Thermo scientific ESCALAB 250 Xi. The samples were prepared by attaching the catalyst particles in the form of thick layer to standard XPS sample carrier block using 10 mm diameter carbon tapes. The base pressure of the chamber was typically in the low 10^{-9} to high 10^{-10} mbar range. Al K_α X-ray was used with a spot size of 650 μm^2. Charge neutralization was used for all samples (1 eV). Spectra were calibrated with respect to C 1s. Quantitative analyses were conducted using the following sensitivity factors with respect to F 1s: Zn $2p_{3/2}$ (4.8), O 1s (0.66), C 1s (0.25), and Au $4f_{7/2}$ (2.8).[30]

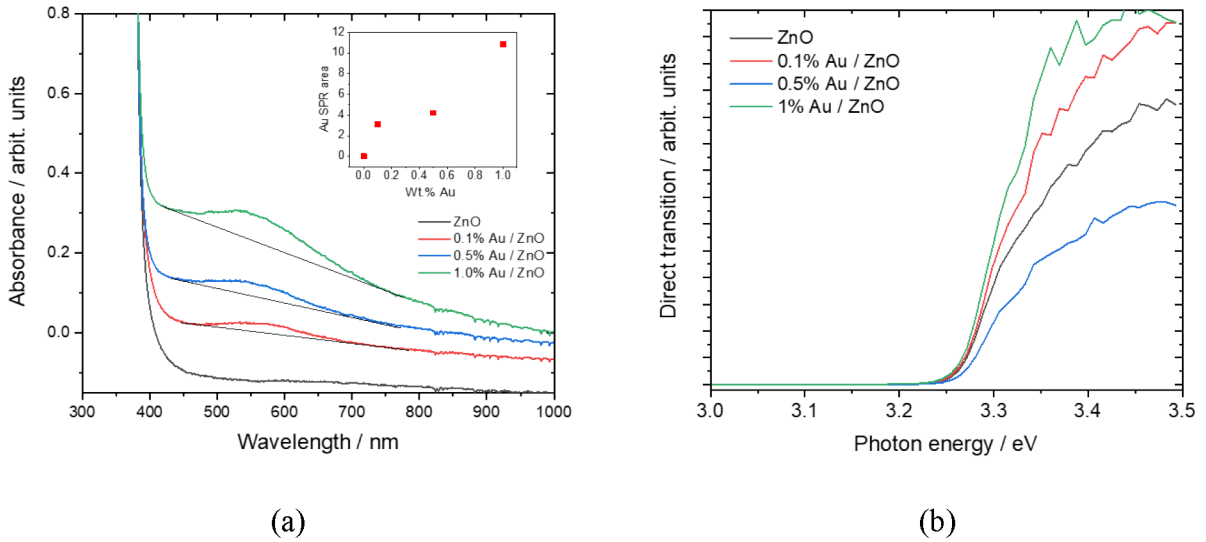

Figure 1. (a) Absorbance spectra and (b) Tauc plots for the Au loaded ZnO powder oxides. LSPR areas were computed following a linear background subtraction, as shown in Figure 1a.

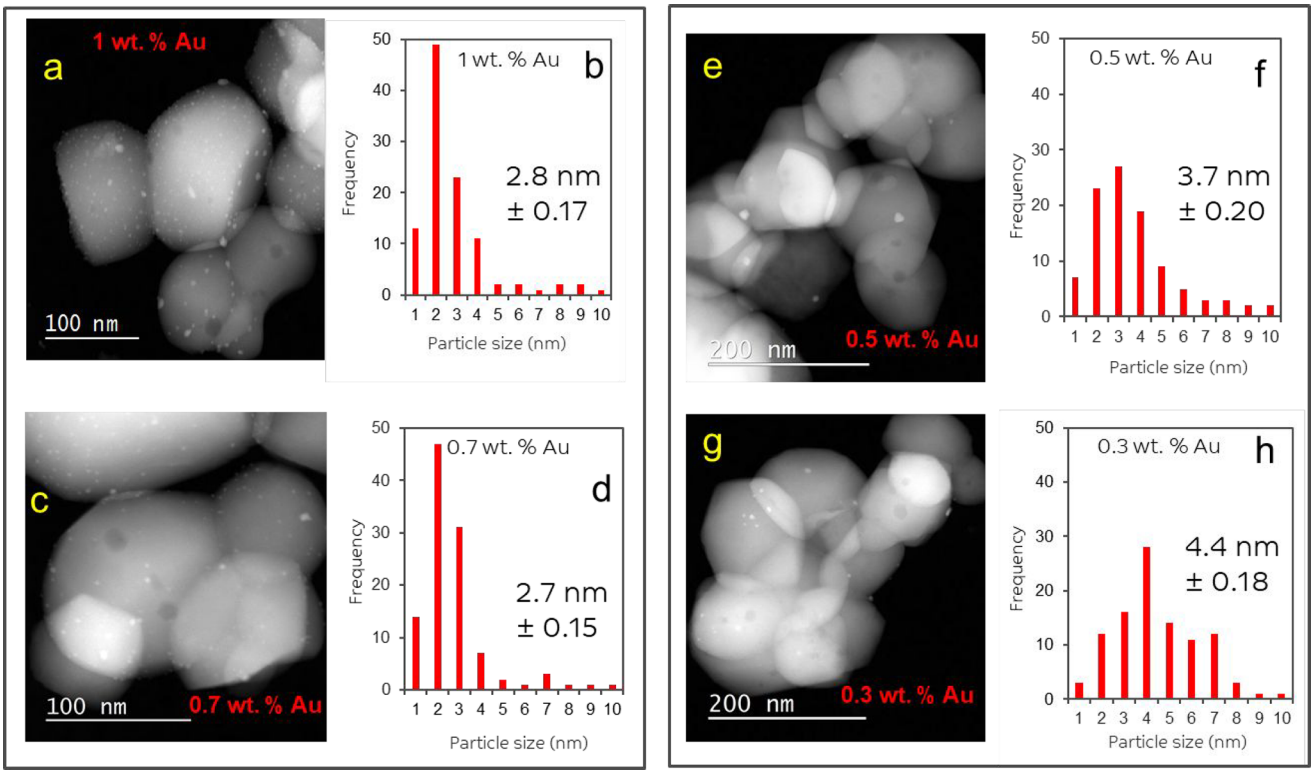

Figure 2. STEM images of *x* wt % Au/ZnO and Au particle size distribution. (a) 1 wt % Au/ZnO; (b) particle size distribution of 1 wt % Au/ZnO; (c) 0.7 wt % Au/ZnO; (d) particle size distribution of 0.7 wt % Au/ZnO; (e) 0.5 wt % Au/ZnO; (f) particle size distribution of 0.5 wt % Au/ZnO; (g) 0.3 wt % Au/ZnO; (h) particle size distribution of 0.3 wt % Au/ZnO.

Photoluminescence (PL) measurements were collected in the range of 300−600 nm using a built on purpose system equipped with a He−Cd laser from Kimmon as the excitation source. The laser emit at 325 nm with a maximum power of 200 mW per spot (about 0.5 cm in size on the sample). The fluorescence is detected trough a Hamamatsu multichannel photomultiplier analyzer (PMA). The distance from the sample and the laser is about 20 cm. The laser beam was further filtered with a pass filter centered on 325 nm to attenuate any parasite emissions from the laser source. The PMA detector is at about 45° from the sample and at a distance of 10 cm. Between the sample and the detector there is a pass filter allowing a range of 340 to 600 nm to eliminate the reflected peak from the incident beam at 325 nm.

Time-resolved photoluminescence (TRPL) spectroscopy measurements were performed using Excipro pump−probe spectrometers (CDP, Moscow). A pulse energy of the fundamental output of a Ti:sapphire fs regenerative amplifier operating at 800 nm with 100 fs pulses and a repetition rate of 1 kHz was used. The pump pulses at 310 and 340 nm were

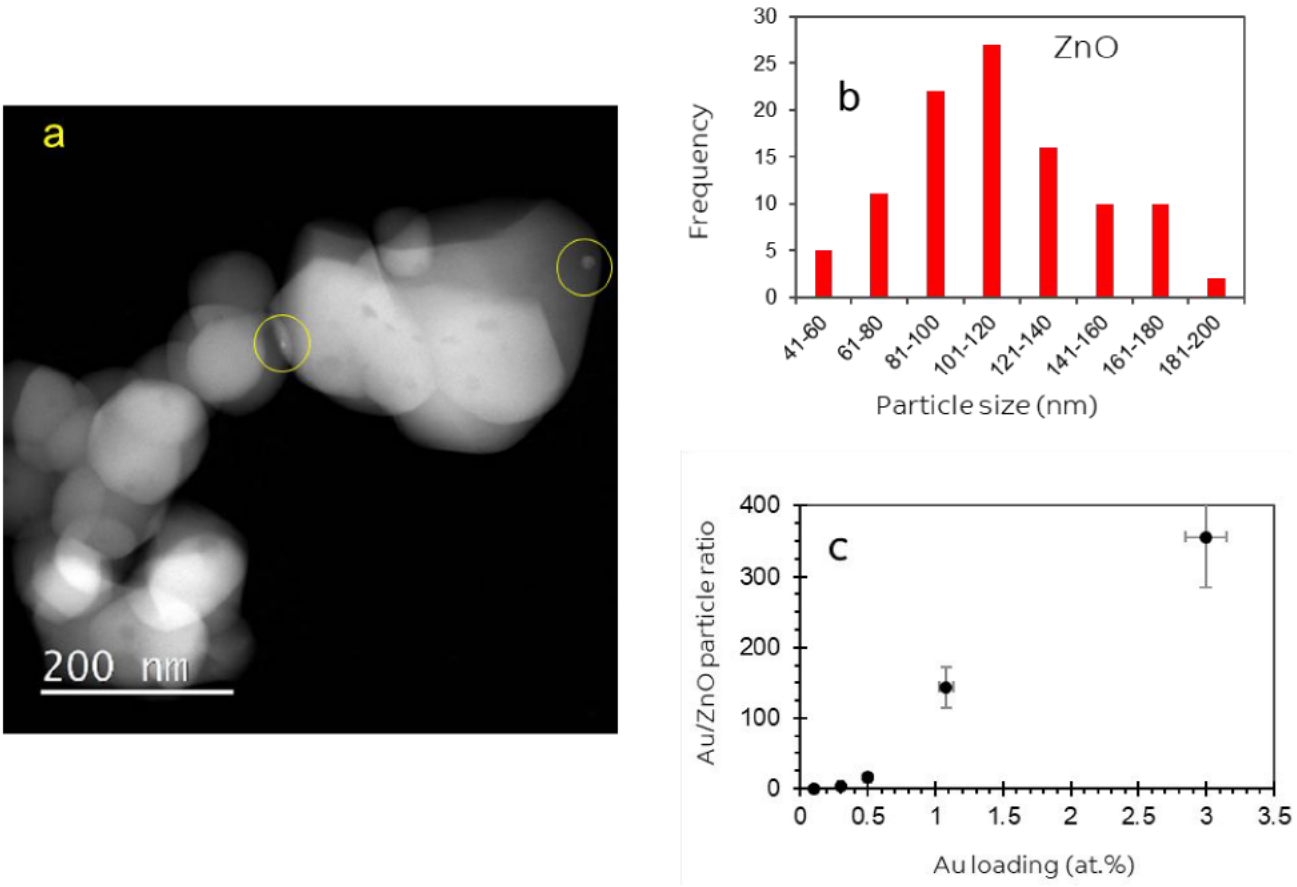

Figure 3. (a) STEM image of 0.1 wt % Au/ZnO; (b) ZnO particle size distribution from STEM images; (c) Au to ZnO particle ratio as a function of Au loading in at.%. Table S1 shows the relation between the weight % and the at.% extracted from XPS Au 4f peak areas (see Figure 4).

created from fs pulses generated in an optical parametric amplifier (TOPAS Prime, Spectra-Physics). To generate the probe pulses (white light) another fraction of the 800 nm amplified pulses was focused onto the 2 mm thick continuously moving CaF_2 crystal. The femtosecond optically gated (FOG) system uses the sum frequency generation nonlinear technique (up-conversion) to obtain the best time resolution. Laser-induced fluorescence (LIF) is produced by the femtosecond laser pulse and directed onto a nonlinear element. Sum frequency radiation (SFR) is generated in the nonlinear element only during the time that a delayed femtosecond gate pulse and fluoresce are temporarily overlapped in the nonlinear crystal. SFR photons were detected by a photomultiplier tube (PMT). The SFR signal is proportional to the florescence signal. Fluorescence kinetics is recorded when the delay between gate and excitation pulses is scanned. Because of the optical delay scanning, the fluorescence decay kinetics was measured at the wavelength determined (from 0 to 1000 ps) by the monochromator and the nonlinear element adjustments.

RESULT AND DISCUSSIONS

Structural and Optical Properties. Figure S1 presents the XRD data of the as prepared ZnO powder with and without Au loading. ZnO exhibits several peaks due to its hexagonal (Wurtzite) phase (JCPDS No. 79−2205), without the presence of other phases. The polycrystalline structure characterized by the presence of lines at 31.8°, 34.4°, 36.3°, 47.6°, 56.6°, 62.9°, 66.3°, 67.9°, 69.1°, and 72.6° corresponding to the (100), (002), (101), (102), (110), (103), (200), (112), (201), and (004) planes is seen, respectively. The corresponding XRD pattern of 1 wt % Au/ZnO (the highest loading of Au used in this study) is also presented in the figure which has the same ZnO pure phase without the detection of gold crystallites.

Figure 1a presents absorbance spectra of ZnO and three Au loaded ZnO. All show an absorbance edge at ca. 380 nm which is at the bandgap energy of ZnO. Figure 1b presents the Tauc plots of the different samples studied. All present a bandgap energy of 3.25 ± 0.05 eV without a noticeable change due to Au loading. Au localized surface plasmon resonance (LSPR) is also seen in Figure 1a in the 500−700 nm range. The signal increases with Au content almost linearly.

Figure 2a−g shows STEM images of the Au/ZnO series as a function of Au loading alongside Au particle size distribution. In the figure, bright spots are those of Au particles because of their much higher mass density when compared to Zn. The particle size distributions (Figure 2b,d,f,h) were obtained using multiple images collected at random locations with measuring a minimum of 100 Au particles in total in each using Gatan software. The assignment of Au particle was further checked using EDX whenever ambiguity aroused. While a large fraction of metal particles are round in shape, others are of different shapes (more images are presented in Figure S2, for the complete series). This is, in particular, noticed at the low loading cases. From the particle size distribution, one notices that their size is smaller at the high loading side and increases with decreasing Au coverage. We have further analyzed, using

high resolution TEM/FFT (fast Fourier transform), Au particles on ZnO for the 1 wt % sample. As seen in Figure S2, it appears that Au particles have their (111) plane aligned at about 18° from the dominant nonpolar plane (101 bar0) of ZnO.

The mean particle size is given in the inset in each graph (b, d, f, and h). The relation between the wt % and at.% (as extracted from XPS Au 4f peak areas) is given in Table S1, see Figure 4 for more details.

Very few particles are noticed in the case of 0.1 wt % loading making it difficult to extract with reasonable accuracy their sizes. Based on the Au particles detected, the mean size was found to be around 7.5 nm much. It is worth noting that despite their very low number they do have a clear LSPR signal (Figure 1a) and that is probably in line with their larger size. The increase of the number of Au particles per ZnO particle ranges from about one Au particle for five ZnO particles, for 0.1 at. % (0.1 wt %), to about 360 Au particles per ZnO particle, for 3 at.% (1.0 wt %) Au/ZnO (Figure 3a–c). The individual size of ZnO particles range from 100 to 120 nm in size with mean particle size of about 105 nm (Figure 3b). ZnO particles seem, however, not to be separated, but fused together, and this may have implications on the charge transfer in the bulk.

To further probe into Au dispersion on ZnO, XPS of the same series was conducted. This is important for further quantification of the luminescence signal. Because e-h recombination may occur in the bulk, far away from the surface, those at (2D) and close to the surface (3D) would be most affected by Au presence. Spectra are referenced to XPS C 1s of adventitious surface carbon at 284.7 eV. XPS Zn 2p, Zn 3p, O 1s, and Au 4f were monitored and quantified. There is an overlap between the XPS Zn $3p_{3/2}$ and Au $4f_{5/2}$, as shown in Figure 4. Quantification is therefore conducted using the Au $4f_{7/2}$ peak area. Furthermore, a ratio is made with respect to Zn 2p to avoid further complication due to the unavoidable presence of adventitious carbon. The empirical sensitivity factor of 2.8 for the peak area of Au $4f_{7/2}$ and of 4.8 for the peak area of Zn $2p_{3/2}$ (with respect to XPS F 1s) were taken (see Experimental Section). As seen in Figure 4, there is no shift in the binding energy of Au $4f_{7/2}$ (at 83.8 ± 0.1 eV) with increased loading. At high loading the Au $4f_{5/2}$ can be noticed at the low binding energy side of XPS Zn $3p_{3/2}$ peak. The difference between Au $4f_{7/2}$ and Au $4f_{5/2}$ binding energies (ΔE = 3.6 eV) together with their binding energy positions indicate that Au atoms are present in all cases on the surface in their metallic (Au^0) state.

Photoluminescence. Figure 5a,b shows photoluminescence spectra of the Au/ZnO series. All presents the two characteristic emission peaks in the UV (380 nm) and visible (550 nm) regions of ZnO. The visible luminescence is more pronounced and much wider than the UV one. The visible luminescence has multiple origins, as indicated in the Introduction. Because of its sensitivity to, in particular, surface and bulk oxygen vacancies in ZnO it is prone to changes of the environment and therefore more complex to study ex situ. Here we focus on the UV emission of the series. Quantitative analyses are presented in Figure 5b in which the signal intensity of the 380 nm emission is plotted as a function of the Au atomic % (as obtained from XPS) of the oxide series. Because gold particles are present on the surface of ZnO particles, it is more accurate to consider the atomic %, as determined from XPS than the nominal ones. The presence of

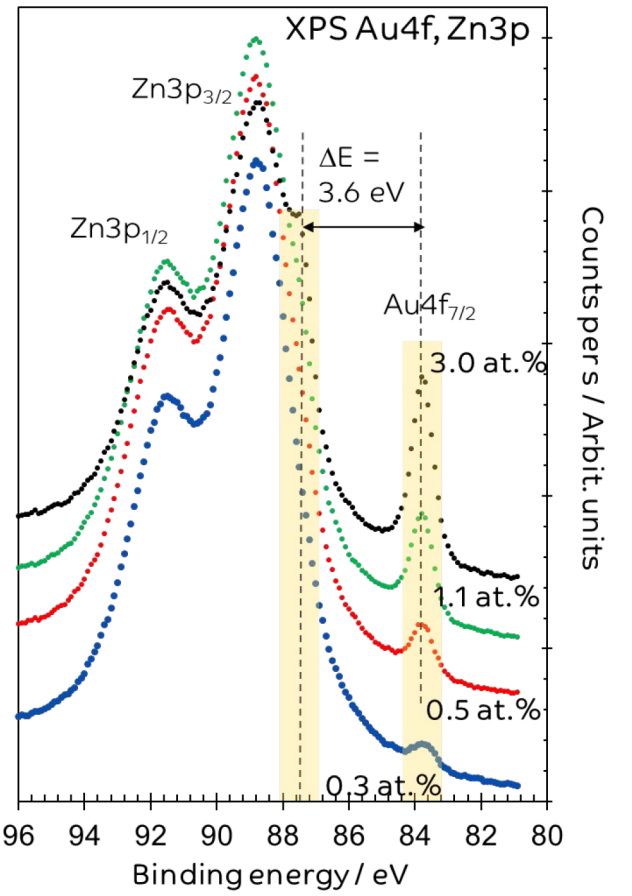

Figure 4. XPS (Zn 3p, Au 4f) of the Au/ZnO series in which Au wt % are 0.3 (blue), 0.5 (red), 0.7 (green), and 1 (black) of the as-prepared oxides. The computed atomic % are indicated on each signal; ΔE = Au $4f_{5/2}$ − Au $4f_{7/2}$ in eV. See Table S1 for the relation between wt % and at.%.

Au, even at the level of 0.1 at.%, decreases the UV signal by about 40%. Further increase of Au at.% resulted in further, but less pronounced, decrease of the UV signal. For example, increasing Au loading on the surface 30 times (3 at.% Au) only doubled the UV signal attenuation (when compared to that of the 0.1 at.% Au).

Time-Resolved Photoluminescence (TPRL). The fact that Au particles change the band to band electron–hole recombination rate can be explained as due to electron transfer from the CB of ZnO to Au particles due to their work function difference. This would be dependent on a few factors: (i) Au coverage, (ii) the diffusion length of excited electrons (and holes), and (iii) the number of excited electrons each particle can hold. Time-resolved spectroscopy at the ps range may probe into the electron transfer between ZnO and Au particles upon monitoring the luminescence of the former.

Figure 6 presents the effect of excitation power on the UV emission signal of ZnO. The power indicated is per light spot which is about 0.1 mm in diameter. In the figure the signal at 385 nm (slightly away from the peak maximum) was monitored as a function of time in ps at the indicated power. The signal decay rate decreases with decreasing the pump power. The faster decay rate with increasing power is due to the effect of high light intensity on the PL that includes lasing, heat, and an increase of the nonradiative recombination fraction, among other factors,[31,32] and is not a focus in the

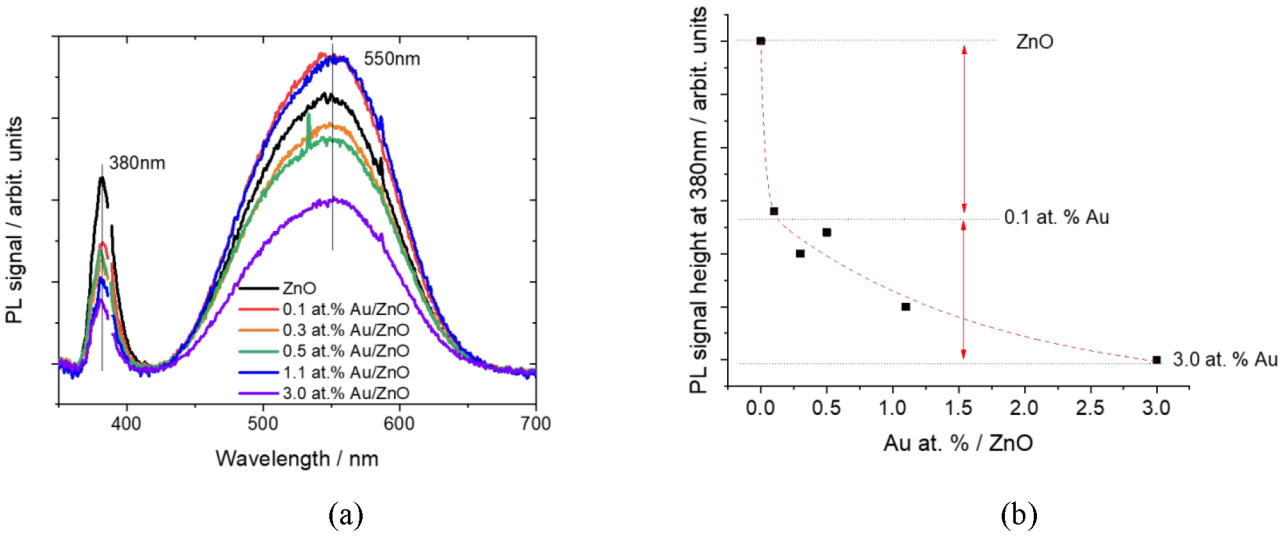

Figure 5. (a) Photoluminescence spectra of the Au/ZnO series at the indicted Au wt % of the as prepared oxides. (b) Signal height intensity of the PL at 380 nm as a function of the Au at.% on ZnO. The correspondence between the nominal wt % and the surface atom % of Au is given in Table S1. The vertical arrows represent the magnitude of the signal decrease with increasing Au atoms.

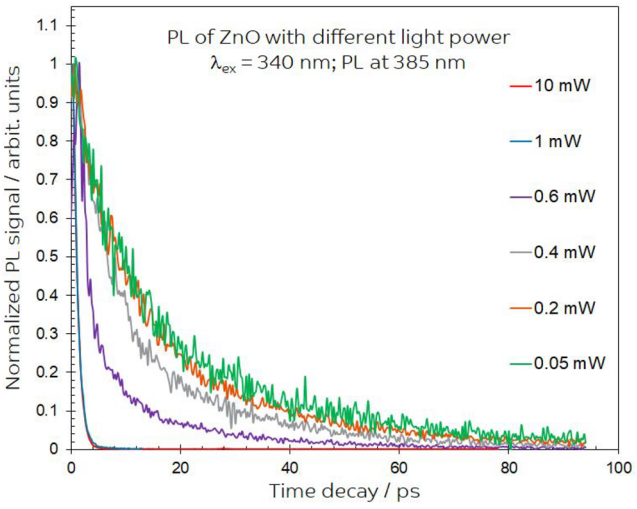

Figure 6. Time-resolved photoluminescence (TPRL) of pure ZnO powder at 385 nm at different excitation power from 10 to 0.05 mW per spot. Excitation light wavelength = 340 nm.

present study. The main observation is that the signals at 0.05 and 0.2 mW are similar, which was considered adequate to use while keeping a good signal-to-noise ratio. Following this we have monitored, using 0.2 mW, the signal in the UV and vis regions to see for possible changes in the decay rates within the same luminescence peak. As seen in Figure 7a,b, there is a range where no changes occur. This is in the 375−385 nm range of the UV emission and in the 480−500 nm range in the visible emission. Thus, we have used this wavelength range for the comparative study between ZnO and Au/ZnO.

Figure 8 shows the decay of the 385 nm signal of the complete series containing Au, with an improved signal-to-noise ratio that allowed using a power of 0.073 mW. The decay rate increases with increasing Au content and this can be best seen by the curvature of the profiles at about 100 ps. Many authors have found that the TRPL signal of ZnO could be fit with a biexponential decay function.[33] The exact meaning of this is still under study and each may not be attributed to a unique physical property. While some authors gave evidence that the two-decay (or life) time t_1 and t_2 are related to bound and free excitons (e-h),[34,35] the exciton has a dissociation energy of about 60 meV,[36] others have attributed them to nonradiative (quench of the luminescence due to phonon interaction) and radiative (CB to VB e-h recombination) decay, respectively.[37] Still others have linked the decay to surface-mediated e-h recombination events.[38] A biexponential function with $R^2 = 0.99$ was obtained for all traces. Fitting the decay rate with a single exponential function was not adequate (see Figure S3), triexponential function was possible with the same R^2 as for the biexponential fit, but gave no further clarity on the data. The results are shown in Table 1. Yet, there is no trend to be noticed. While the mean lifetime, $\langle t \rangle$, initially decreased, it increased again then decreased further.

To further probe into the effect of Au, we opted to integrate the emission from each oxide (number of photons × time) with the difference between them traced to the presence of Au. Figure 9a presents the integral function of the biexponential decay function for the Au/ZnO series.

It is seen that the fraction of photons emitted up to about 20 ps has an equal contribution in each sample. This may mean that the emission up to this time is not related to the presence of Au on top of ZnO particles. After which, a deviation occurred that has accentuated with time. While a trend is observed in which the integrated signals get smaller with increasing Au content (with the exception of the 0.3 wt %), further quantification nominally including Au atoms would be needed. Figure 9b presents the change in the value of the integrated signal before and after normalization to the number of atoms of Au (in %) as a function of Au at.%.

The normalized values represent the quenching power per gold atom (or %) on top of the excited semiconductor. This quenching can be linked to the trapping of CB electrons by gold particles. The data can be fit with a single exponential function with respect to Au content ($y(x) = A \exp(-ax)$). The value a (2.4 approximated to 2) may not have a direct physical meaning yet since x is effectively the "number of photons in a unit time divided by the number of atoms of gold", the value of two may indicate that each gold atom prevents two photons from being emitted by quenching two electrons from the

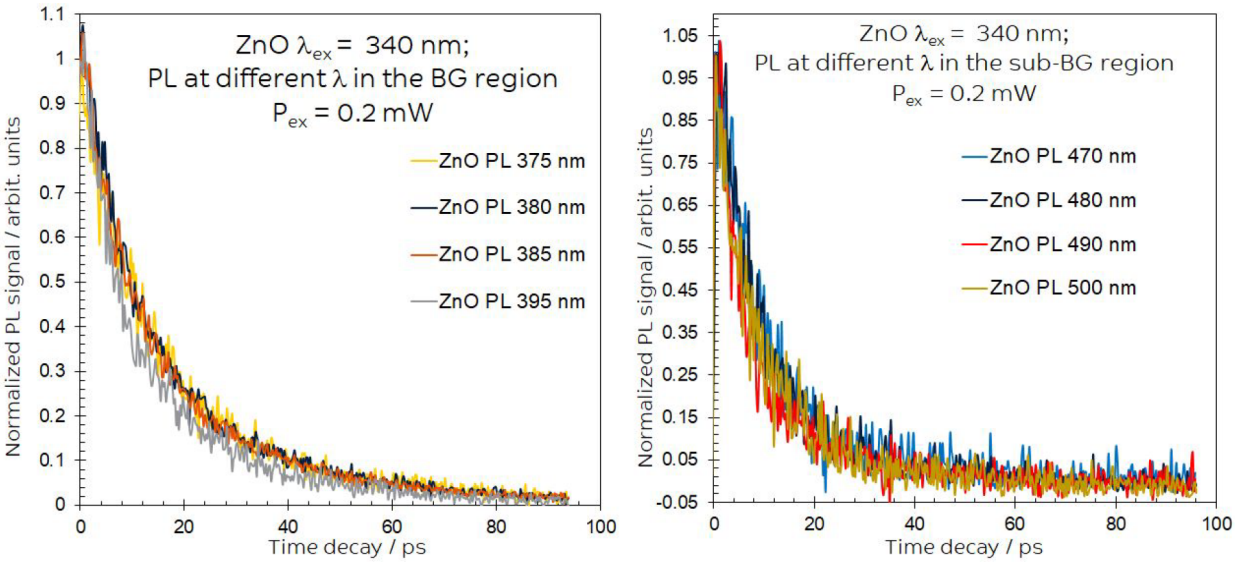

Figure 7. Time-resolved photoluminescence (TPRL) of pure ZnO powder of the UV (a) and visible (b) emissions at different wavelengths. Excitation light wavelength = 340 nm; Excitation light power = 0.2 mW/spot.

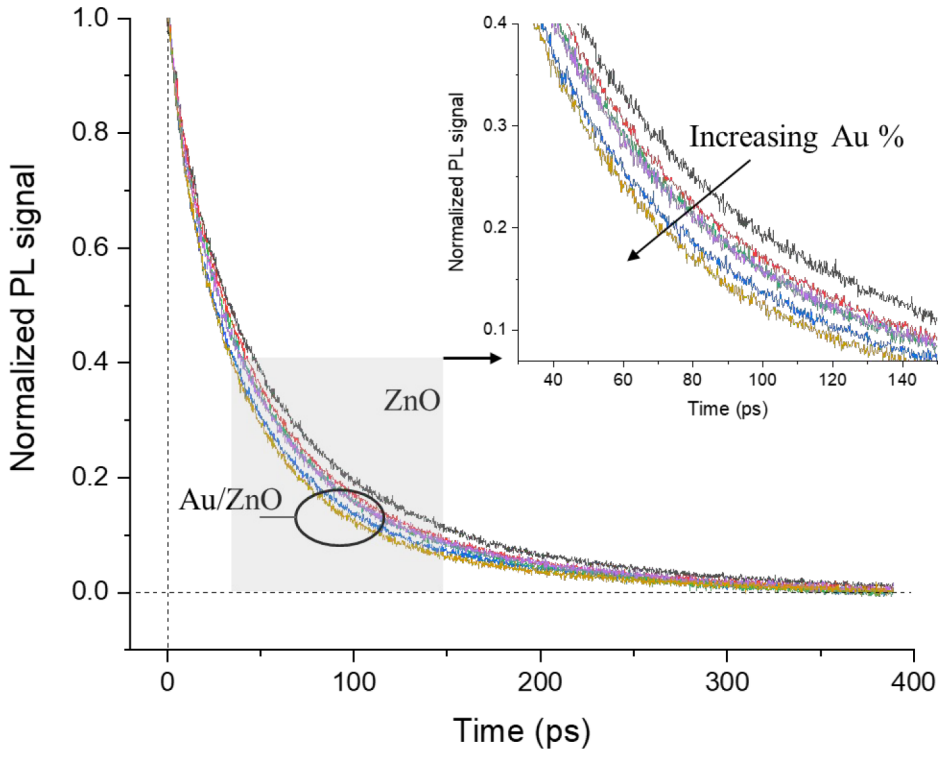

Figure 8. Normalized time-resolved photoluminescence (TPRL) of the Au/ZnO series of the UV emission. The inset is an enlarged area in the 30−160 ps range. The spectra for the 0.5 and 0.7 wt % gold had a linear background subtraction of about 0.03.

conduction band. Moreover, the exponential decay does indicate that, while adding more Au atoms increases the e-h recombination rate, the overall efficiency, per Au atom, of the system has decreased. If all Au particles affected independently the electron transfer rate, their effect would be linear. This observation is similar, albeit in a different field, to many observations related to the effect of metal coverage on n-type semiconductors on their photoreaction for hydrogen ions reduction to molecular hydrogen.[39−43] In all this work there is a small window in which the catalysts have a high activity and that is typically in the 1−2 wt % range (which is about 0.5 at.% of Au deposited on 3d oxide semiconductors).

Increasing Au coverage on the surface results in decreasing the interparticle distance in general. The following explanation may then be postulated. Au particles of a few nm in size absorb UV light.[44,45] This may then create high energy electrons that leak back into the semiconductor (ZnO). This, in turn, would increase the electron density at the interface Au/ZnO. This would repel the excited electrons transfer rate from ZnO to Au and, thus, "collectively" decrease the trapping efficiency per particle. Because the excited electron diffusion length in ZnO is

Table 1. Lifetime, t_1 and t_2, and Amplitudes (Prefactors), A_1 and A_2, of the Fitted Biexponential Functions of the 385 nm Signal for the Au/ZnO Series[a]

oxide	t_1 (ps) 385 nm	(A_1)	t_2 (ps) 385 nm	(A_2)	$\langle t \rangle$ (10^{-12} s)	k (10^{10} s^{-1})	Δk (10^{10} s^{-1})
ZnO	21.90	0.40	85.0	0.60	75.8	1.32	
0.1 wt % Au (0.1 at.%)	21.80	0.41	77.50	0.59	68.4	1.46	0.14
0.3 wt % Au (0.3 at.%)	20.40	0.55	76.80	0.45	63.1	1.58	0.26
0.5 wt % Au (0.5 at.%)	24.00	0.50	92.50	0.50	78.4	1.28	−0.04
0.7 wt % Au (1.1 at.%)	24.70	0.55	103.0	0.45	85.4	1.17	−0.15
1.0 wt % Au (3.0 at.%)	20.00	0.53	69.0	0.47	56.9	1.76	0.44

[a]Mean lifetime $\left\langle t \right\rangle = \frac{\sum(A_i \times t_i^2)}{\sum(A_i \times t_i)}$; $k = 1/\langle t \rangle$; $\Delta k = k_{Au/ZnO} - k_{ZnO}$.

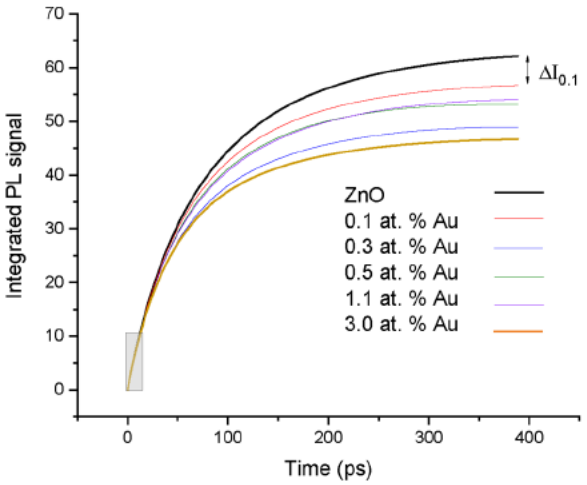

(a)

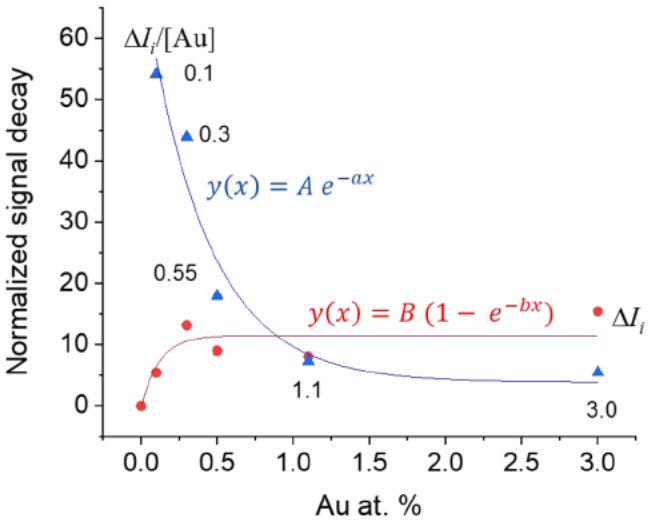

(b)

Figure 9. (a) Integration of the fitted curves of Figure 8 for the Au/ZnO series to highlight the effect of Au in quenching the UV emission; the highlighted area near the origin is extended in Figure S4. (b) The difference in the total integrated areas between pure ZnO and Au/ZnO before (red circles) and after (blue triangles) normalization to the content of Au in at.%. ΔI_i is the difference between the integrated signal of pure ZnO and that of Au/ZnO, with i being the atomic %.

much larger than the interparticle separation length, the electrons might be scattered away from Au particles when the density of the latter increases.

CONCLUSIONS

Time-resolved photoluminescence (TRPL) was conducted on a Au/ZnO series with Au at.% between 0.1 and 3.0. The mean Au particle size was 2.7−4.4 nm in size when deposited on ZnO particles of about 100 nm in size. All Au-containing materials showed a pronounced surface plasmon resonance signal (SPR) at about 2.5 eV. The band-to-band (e-h) recombination on ZnO and Au/ZnO signal decay, monitored by TRPL, was best fitted with a biexponential function with time constants t_1 and t_2 ranging from 20 to 25 ps and from 57 to 85 ps, respectively. The presence of Au particles decreased the signal (increased the decay rate) in all cases. Extracting quantitative information was made possible upon normalization of the integrated decay signal, over the investigated time domain, with gold atoms as obtained from XPS Au $4f_{7/2}$/Zn $2p_{3/2}$. The extracted data were best fitted with a single exponential decay function with respect to Au atoms on the surface of ZnO; $y(x) = A \exp(-ax)$, where x is the at.% of Au on ZnO and $a = 1.8$. This might indicate that each Au atom can pump away up to two electrons from the conduction band (CB). The overall trapping efficiency, however, decreased with increasing Au coverage considerably. This can be related to the Au particles' response to light where the created hot electrons at the interface with ZnO scatter away CB electrons and therefore decrease their trapping efficiency per atom of gold. It is therefore postulated that the interparticle distance of the plasmonic metal on an excited semiconductor may have a pronouced role on the overall charge transfer kinetics.

ASSOCIATED CONTENT

Supporting Information

The Supporting Information is available free of charge at https://pubs.acs.org/doi/10.1021/acs.jpcc.2c04005.

XRD diagrams of ZnO and Au/ZnO powder. STEM and TEM images of the Au/ZnO together with FFT of ZnO and Au TEM images. A representative fitting of the time-resolved PL of one Au/ZnO sample to highlight the difference between single and biexponential functions. Au weight % on ZnO series, together with their nominal at.% and the at.% extracted from XPS Au 4f peak areas. Integrated areas of the time-resolved PL of the Au/ZnO series (PDF)

AUTHOR INFORMATION

Corresponding Author

H. Idriss − *Institute of Functional Interfaces (IFG), Karlsruhe Institute of Technology (KIT), 76344 Karlsruhe, Germany;* orcid.org/0000-0001-8614-7019; Email: hicham.idriss@kit.edu

Authors

A. Ziani − *Surface Science and Advanced Characterisation, SABIC Corporate Research Center at KAUST, Thuwal 21961, Saudi Arabia*

S. Al-Taweel − *Surface Science and Advanced Characterisation, SABIC Corporate Research Center at KAUST, Thuwal 21961, Saudi Arabia*

M. A. Nadeem − *Surface Science and Advanced Characterisation, SABIC Corporate Research Center at KAUST, Thuwal 21961, Saudi Arabia*

Notes

The authors declare no competing financial interest.

ACKNOWLEDGMENTS

H.I. thanks the German Research Foundation (DFG), Project number 426888090, SFB 1441. The authors thank Dr. T. Ahmed at SABIC R&D (Riyadh, Saudi Arabia) for conducting the XPS measurements.

REFERENCES

(1) Djurîšić, A. B.; Leung, Y. H. Optical properties of ZnO nanostructures. *Small* **2006**, *2*, 944−961.

(2) Djurîšić, A. B.; Ng, A. M. C.; Chen, X. Y. ZnO nanostructures for optoelectronics: Material properties and device applications. *Prog. Quantum Electron.* **2010**, *34*, 191−259.

(3) Fujii, K.; Goto, T.; Yao, T. Properties of ultraviolet anti-Stokes photoluminescence in ZnO single crystals. *Phys. Status Solidi A* **2012**, *209*, 761−765.

(4) Yoneta, M.; Yoshino, K.; Ohishi, M.; Saito, H. Photoluminescence studies of high-quality ZnO single crystals by hydrothermal method. *Phys. B: Condens. Matt.* **2006**, *376*−*377*, 745−748.

(5) Zabels, R.; Muktepavela, F.; Grigorjeva, L.; Tamanis, E.; Mishels-Piesins, M. Nanoindentation and photoluminescence characterization of ZnO thin films and single crystals. *Opt. Mater.* **2010**, *32*, 818−822.

(6) Feng, L.; Cheng, C.; Yao, B. D.; Wang, N.; Loy, M. M. T. Photoluminescence study of single ZnO nanostructures: Size effect. *Appl. Phys. Lett.* **2009**, *95*, 053113.

(7) Idriss, H.; Andrews, R. M.; Barteau, M. A. Application of luminescence techniques to probe surface−adsorbate interactions on oxide single crystals. *J. Vac. Sci. Technol. A* **1993**, *11*, 209−218.

(8) Idriss, H.; Barteau, M. A. Photoluminescence from zinc oxide powder to probe adsorption and reaction of O_2, CO, H_2, HCOOH, and CH_3OH. *J. Phys. Chem.* **1992**, *96*, 3382−3388.

(9) Cohn, A. W.; Janßen, N.; Mayer, J. M.; Gamelin, D. R. Photocharging ZnO nanocrystals: picosecond hole capture, electron accumulation, and Auger recombination. *J. Phys. Chem. C* **2012**, *116*, 20633−20642.

(10) Xiong, G.; Pal, U.; Serrano, J. G. Correlations among size, defects, and photoluminescence in ZnO nanoparticles. *J. Appl. Phys.* **2007**, *101*, 024317.

(11) Han, X.; Wang, G.; Wang, Q.; Cao, L.; Liu, R.; Zou, B.; Hou, J. G. Ultraviolet lasing and time-resolved photoluminescence of well-aligned ZnO nanorod arrays. *Appl. Phys. Lett.* **2005**, *86*, 223106.

(12) Demille, T. B.; Hughes, R. A.; Preston, A. S.; Adelung, R.; Mishra, Y. K.; Neretina, S. Light-mediated growth of noble metal nanostructures (Au, Ag, Cu, Pt, Pd, Ru, Ir, Rh) from micro- and nanoscale ZnO tetrapodal backbones. *Front. Chem.* **2018**, *6*, 1−8.

(13) Li, W.; Hua, F.; Yue, J.; Li, J. L. Ag@AgCl Plasmon-induced sensitized zno particle for high-efficiency photocatalytic property under visible light. *Appl. Surf. Sci.* **2013**, *285*, 490−497.

(14) Bertoni, G.; Fabbri, F.; Villani, M.; Lazzarini, L.; Turner, S.; Van Tendeloo, G.; Calestani, D.; Gradečak, S.; Zappettini, A.; Salviati, G. Nanoscale mapping of plasmon and exciton in ZnO tetrapods coupled with au nanoparticles. *Sci. Rep.* **2016**, *6*, 19168.

(15) Jia, C.; Zhong, W.; Deng, M.; Jiang, J. Microscopic insight into the activation of O_2 by Au nanoparticles on ZnO(101) support. *J. Phys. Chem. C* **2016**, *120*, 4322−4328.

(16) Chiu, Y.-H.; Chang, K.-D.; Hsu, Y.-J. Plasmon-mediated charge dynamics and photoactivity enhancement for Au-decorated ZnO nanocrystals. *J. Mater. Chem. A* **2018**, *6*, 4286−4296.

(17) Zhou, N.; Zhu, H.; Li, S.; Yang, J.; Zhao, T.; Li, Y.; Xu, Q.-H. Au Nanorod/ZnO core−shell nanoparticles as nano-photosensitizers for near-infrared light-induced singlet oxygen generation. *J. Phys. Chem. C* **2018**, *122*, 7824−7830.

(18) Liu, K. W.; Tang, Y. D.; Cong, C. X.; Sum, T. C.; Huan, A. C. H.; Shen, Z. X.; Wang, L.; Jiang, F. Y.; Sun, X. W.; Sun, H. D. Giant enhancement of top emission from ZnO thin film by nanopatterned Pt. *Appl. Phys. Lett.* **2009**, *94*, 151102.

(19) Fiedler, S.; Lem, L. O. L. C.; Ton-That, C.; Hoffmann, A.; Phillips, M. R. Enhancement of the UV emission from gold/ZnO nanorods exhibiting no green luminescence. *Opt. Mater. Express* **2020**, *10*, 1476−1487.

(20) Burda, C.; Chen, X.; Narayanan, R.; El-Sayed, M. A. Chemistry and properties of nanocrystals of different shapes. *Chem. Rev.* **2005**, *105*, 1025−1102.

(21) Sakurai, M.; Liu, K.; Ceolato, R.; Aono, M. Optical properties of ZnO nanowires decorated with Au nanoparticles. *Key Eng. Mater.* **2013**, *547*, 7−10.

(22) Lee, J.; Shim, H. S.; Lee, M.; Song, J. K.; Lee, D. Size-controlled electron transfer and photocatalytic activity of ZnO-Au nanoparticle composites. *J. Phys. Chem. Lett.* **2011**, *2*, 2840−2845.

(23) Park, J.; Deshmukh, P. R.; Sohn, Y.; Shin, W. G. ZnO-TiO_2 core-shell nanowires decorated with Au nanoparticles for plasmon-enhanced photoelectrochemical water splitting. *J. Alloys Compd.* **2019**, *787*, 1310−1319.

(24) Udawatte, N.; Lee, M.; Kim, J.; Lee, D. Well-defined Au/ZnO nanoparticle composites exhibiting enhanced photocatalytic activities. *ACS Appl. Mater. Interfaces* **2011**, *3*, 4531−4538.

(25) Bahariqushchi, R.; Cosentino, S.; Scuderi, M.; Dumons, E.; Tran-Huu-Hue, L. P.; Strano, V.; Grandjean, D.; Lievens, P.; Poulin-Vittrant, P.; Spinella, C.; et al. Free carrier enhanced depletion in ZnO nanorods decorated with bimetallic AuPt nanoclusters. *Nanoscale* **2020**, *12*, 19213−19222.

(26) Zanella, R.; Giorgio, S.; Henry, C. R.; Louis, C. Alternative methods for the preparation of gold nanoparticles supported on TiO_2. *J. Phys. Chem. B* **2002**, *106*, 7634−7642.

(27) Alonso, F.; Riente, P.; Rodríguez-Reinoso, F.; Ruiz-Martínez, J.; Sepúlveda-Escribano, A.; Yus, M. Platinum nanoparticles supported on titania as an efficient hydrogen-transfer catalyst. *J. Catal.* **2008**, *260*, 113−118.

(28) Kubelka, D.; Munk, L. Ein beitrag zur optik der farbanstriche. *Z. Technol. Phys.* **1931**, *12*, 593−601.

(29) Wahab, A. K.; Nadeem, M. A.; Idriss, H. Hydrogen Production During Ethylene Glycol Photoreactions Over Ag-Pd/TiO2 at Different Partial Pressures of Oxygen. *Front. Chem.* **2019**, *7*, No. 780.

(30) Wagner, C. D.; Davis, L. E.; Zeller, M. V.; Taylor, J. A.; Raymond, R. M.; Gale, L. H. Empirical atomic sensitivity factors for quantitative analysis by electron spectroscopy for chemical analysis. *Surf. Interface Anal.* **1981**, *3*, 211−225.

(31) Kwok, W. M.; Djurîšić, A. B.; Leung, Y. H.; Chan, W. K.; Phillips, D. L.; Chen, H. Y.; Wu, C. L.; Gwo, S.; Xie, M. H. Study of excitonic emission in highly faceted ZnO rods. *Chem. Phys. Lett.* **2005**, *412*, 141−144.

(32) Djurîŝić, A. B.; Kwok, W. M.; Leung, Y. H.; Chan, W. K.; Phillips, D. L. Stimulated emission in ZnO nanostructures: A Time-resolved study. *J. Phys. Chem. B* **2005**, *109*, 19228−19233.
(33) Han, X.; Wang, G.; Wang, Q.; Cao, L.; Liu, R.; Zou, B.; Hou, J. G. Ultraviolet lasing and time-resolved photoluminescence of well-aligned ZnO nanorod arrays. *Appl. Phys. Lett.* **2005**, *86*, 223106.
(34) Teke, A.; Ozgur, U.; Dogan, S.; Gu, X.; Morkoc, H.; Nemeth, B.; Nause, J.; Everitt, H. O. Excitonic fine structure and recombination dynamics in single-crystalline ZnO. *Phys. Rev. B* **2004**, *70*, 195207.
(35) Chen, S. Excitonic effects and energy upconversion in bulk and nanostructured ZnO. *Linköping Studies in Science and Technology Dissertation*, Linköping University, The Institute of Technology, 2014..
(36) Huang, M. H.; Mao, S.; Feick, H.; Yan, H.; Wu, Y.; Kind, H.; Weber, E.; Russo, R.; Yang, P. Room-temperature ultraviolet nanowire nanolasers. *Science* **2001**, *292* (8), 1897−1899.
(37) van Dijken, A.; Meulenkamp, E. A.; Vanmaekelbergh, D.; Meijerink, A. The kinetics of the radiative and nonradiative processes in nanocrystalline ZnO particles upon photoexcitation. *Phys. Chem. B* **2000**, *104*, 1715−1723.
(38) Li, M.; Xing, G.; Ah Qune, L. F. N.; Xing, G.; Wu, T.; Huan, C. H. A.; Zhang, X.; Sum, T. C. Tailoring the charge carrier dynamics in ZnO nanowires: the role of surface hole/electron traps. *Phys. Chem. Chem. Phys.* **2012**, *14*, 3075−3082.
(39) Al-Azri, Z. H.N.; Chen, W.-T.; Chan, A.; Jovic, V.; Ina, T.; Idriss, H.; Waterhouse, G. I.N. The roles of metal co-catalysts and reaction media in photocatalytic hydrogen production: Performance evaluation of M/TiO_2 photocatalysts (M = Pd, Pt, Au) in different alcohol-water mixtures. *J. Catal.* **2015**, *329*, 355−367.
(40) Bamwenda, G. R.; Tsubota, S.; Nakamura, T.; Haruta, M. Photoassisted hydrogen production from a water-ethanol solution: a comparison of activities of Au-TiO_2 and Pt-TiO_2. *J. Photochemi. Photobiol. A: Chem.* **1995**, *89*, 177−189.
(41) Bowker, M.; Bahruji, H.; Kennedy, J.; Jones, W.; Hartley, G.; Morton, C. The photocatalytic window: photo-reforming of organics and water splitting for sustainable hydrogen production. *Catal. Lett.* **2015**, *145*, 214−219.
(42) Berr, M. J.; Schweinberger, F. F.; Döblinger, M.; Sanwald, K. E.; Wolff, C.; Breimeier, J.; Crampton, A. S.; Ridge, C. J.; Tschurl, M.; Heiz, U.; et al. J. Size-selected subnanometer cluster catalysts on semiconductor nanocrystal films for atomic scale insight into photocatalysis. *Nano Lett.* **2012**, *12*, 5903−5906.
(43) Katsiev, K.; Harrison, G.; Al-Salik, Y.; Thornton, G.; Idriss, H. Gold cluster coverage effect on H_2 production over rutile TiO_2(110). *ACS Catal.* **2019**, *9*, 8294−8305.
(44) Wey, K.; Epple, M. Ultrasmall gold and silver/gold nanoparticles (2 nm) as autofluorescent labels for poly(D,L-lactide-*co*-glycolide) nanoparticles (140 nm). *J. Mater. Sci.: Mater. Med.* **2020**, *31*, 117.
(45) Zheng, J.; Zhou, C.; Yu, M.; Liu, J. Different sized luminescent gold nanoparticles. *Nanoscale* **2012**, *4*, 4073−4083.